Phase diagram and incommensurate phases in undoped manganites

J. Salafranca and L. Brey
Instituto de Ciencia de Materiales de Madrid (CSIC), Cantoblanco, 28049 Madrid, Spain
(Received 15 September 2005; published 26 January 2006)

We study the existence of incommensurate phases in the phase diagram of the two orbital double exchange model coupled with Jahn-Teller phonons and with superexchange interactions. In agreement with experimental results, we find that undoped manganites $R\mathrm{MnO}_3$ (R being some rare earth element) show temperature induced commensurate-incommensurate phase transitions. In the incommensurate phase the magnetic wave vector varies with temperature. The incommensurate phase arises from the competition between the short range antiferromagnetic superexchange interaction and the long range ferromagnetic double exchange interaction.

DOI: 10.1103/PhysRevB.73.024422 PACS number(s): 75.47.Gk, 75.10.−b, 75.30.−m, 75.50.−y

I. INTRODUCTION

Perovskites of manganese of formula $(R_{1-x}A_x)\mathrm{MnO}_3$ where R denotes rare earth ions ($R=\mathrm{La,Pr,Nd,\ldots}$) and A is a divalent alkaline ion ($A=\mathrm{Ca,Sr,\ldots}$) have attracted a great interest because they show a remarkable colossal magnetoresistance effect at doping x near one-third.[1,2] In these oxides x corresponds to the concentration of holes moving in the e_g orbital bands of the Mn ions that ideally form a cubic structure. From the basic point of view these materials are a challenge for both theoreticians and experimentalists as they show a very rich phase diagram.[3] As function of temperature and hole doping, these systems present orbital, charge or spin order, and in a large portion of the phase diagram these orders coexist.[4–15] Nanophase separation near $x=1/3$ (Ref. 16) and commensurate incommensurate transition near half doping seem to occur in colossal magnetoresistance manganites.[17–20]

Many properties of manganites depend on the competition between the kinetic energy tending to delocalize the carriers and localization effects such as the Jahn-Teller (JT) coupling and the antiferromagnetic (AFM) coupling between the Mn core spins. Therefore the properties of manganites at intermediate doping can be described within a band structure picture, where the itinerant e_g carriers have a strong ferromagnetic interaction with the core t_{2g} Mn spins, and are coupled with the Jahn-Teller distortions of the oxygen octahedra surrounding the Mn ions.[3,15] However, the parent compounds, $R\mathrm{MnO}_3$, are always insulator and their physical properties were typically described in the picture of strongly correlated Mott localized d-electrons.[21–27] However some spin and orbital ordering found experimentally in undoped materials[28–30] cannot be easily described in this picture of strongly localized electrons.

In Ref. 29 the authors examine the magnetic and orbital order in a series of $R\mathrm{MnO}_3$ as a function of the ionic radius (r_R) of the rare earth ion R. For small ionic radius the manganites have a antiferromagnetic spin order of type A coexisting with a $(\pi,\pi,0)$ orbital ordering, whereas for larger values of r_R the magnetic order is of type E. In the A phase, a Mn spin is ferromagnetically coupled with the Mn spins located in the same plane (x-y), and antiferromagnetically with the Mn spins belonging to different planes. In the E phase the x-y layers are antiferromagnetically coupled, but the magnetic structure within the planes is that of ferromagnetic zigzag chains coupled antiferromagnetically. The horizontal (x) and vertical (y) steps of the zigzag chains contain two Mn ions. For values of r_R close to the critical value where the magnetic order changes from A-type to E-type, the manganites develop different magnetic incommensurate phases when increasing temperature. In this reference, assuming perfect orbital order, the problem was mapped into the anisotropic next-nearest-neighbor Ising or ANNNI model.[31] Although this approach provides a phenomelogical explanation of the experimental results, it does not clarify the microscopic origin of the different phases.

It has been suggested recently,[32–34] that the complete nesting between the two e_g bands that occurs in the A structure produces a spin-orbital ordering and opens a gap in the energy spectrum of undoped $R\mathrm{MnO}_3$. Quoting Ref. 34 we do not claim that the real $R\mathrm{MnO}_3$ systems can be fully described by a weak coupling approach as correlation effects can be important, although a treatment based in band structure calculation may be very useful to understand some properties of these materials. In particular, in Ref. 32 using a two orbital double exchange model, it was obtained that the experimental observed E-phase exits in a wide region of parameter space, and it is adjacent to the A-type phase. Coulomb intraorbital interactions might be significant. However, the inclusion of realistic interorbital Coulomb interaction in the microscopic model[3,14] only renomalizes the critical parameters of the phase diagram, maintaining the topology of the diagram unaltered.

One of the issues that remains to be understood is the microscopic origin of the incommensurate phases appearing near the A-type to E-type magnetic transition. The aim of this work is to explain these phases using a realistic microscopic model. The Hamiltonian we study describes electrons moving in two e_g bands, that are ferromagnetically strongly coupled to the Mn core spins as well to the Jahn-Teller phonons. In addition, we also consider a direct superexchange interaction between the core Mn spins. Starting from this Hamiltonian we derive a functional that describes a temperature induced commensurate-incommensurate transition similar to that observed experimentally.

The main result of this work is that near the A to E phase transition, the competition between the nearest-neighbor an-

tiferromagnetic superexchange interaction and the double exchange induced long range ferromagnetic interaction, results in the appearance of incommensurate phases. These phases consist of a periodic array of domain walls.

The rest of the paper is organized as follows. In Sec. II we describe the microscopic model and we present the zero temperature phase diagram. In Sec. III we outline the method for obtaining the critical temperatures and we present the phase diagram composed of the different uniform phases. In Sec. IV we develop the functional for describing spatially modulated phases. Also in Sec. IV we study how the phase diagram of manganites at $x=1$ is altered when soliton incommensurate phases are taken into account. We finish in Sec. V with a brief summary.

II. MICROSCOPIC HAMILTONIAN AND ZERO TEMPERATURE PHASE DIAGRAM

We are interested in the transition between the A and E phases. In these phases the x-y planes are coupled antiferromagnetically and therefore we can analyze the properties of these states and the transition between them by studying a Hamiltonian which describes electrons moving in the x-y plane. The Coulomb interaction between electrons prevents double occupancy and aligns the spins of the d orbitals. The crystal field splits the Mn d levels into an occupied t_{2g} triplet and a doublet of e_g symmetry where $1-x$ electrons per Mn must accommodate. The Hund's coupling between the spins of the e_g electrons and each core spin is much larger than any other energy in the system, and each electron spin is forced to align locally with the core spin texture. Then the e_g electrons can be treated as spinless particles and the hopping amplitude between two Mn ions is modulated by the spin reduction factor,

$$f_{12} = \cos\frac{\vartheta_1}{2}\cos\frac{\vartheta_2}{2} + e^{i(\phi_1-\phi_2)}\sin\frac{\vartheta_1}{2}\sin\frac{\vartheta_2}{2}, \qquad (1)$$

where $\{\vartheta_i, \phi_i\}$ are the Euler angles of the, assumed classical, Mn core spins $\{\mathbf{S}_i\}$. This is the so-called double exchange (DE) model.[35–37]

We study a double exchange model coupled to Jahn-Teller (JT) phonons. We also include the antiferromagnetic coupling between the Mn core spins J_{AF},

$$H = -\sum_{i,j,a,a'} f_{i,j} t^{u}_{a,a'} C^{+}_{i,a} C_{j,a'} + J_{AF}\sum_{\langle i,j\rangle} \mathbf{S}_i \mathbf{S}_j + \frac{1}{2}\sum_i (\beta Q^2_{1i} + Q^2_{2i} + Q^2_{3i}) + \lambda \sum_i (Q_{1i}\rho_i + Q_{2i}\tau_{xi} + Q_{3i}\tau_{zi}), \qquad (2)$$

here $C^{+}_{i,a}$ creates an electron in the Mn ion located at site i, in the e_g orbital a ($a=1,2$ with $1=|x^2-y^2\rangle$ and $2=|3z^2-r^2\rangle$). The hopping amplitude $t_{aa'}$ is finite for next neighbors Mn and depends both on the type of orbital involved and on the direction u between sites i and j ($t^{x(y)}_{1,1} = \pm\sqrt{3}t^{x(y)}_{1,2} = \pm\sqrt{3}t^{x(y)}_{2,1} = 3t^{x(y)}_{2,2} = t$)[3]. t is taken as the energy unit. The fourth term couples the e_g electrons with the three active MnO_6 octahedra distortions: the breathing mode Q_{1i}, and the JT modes Q_{2i} and Q_{3i} that have symmetry x^2-y^2 and $3z^2-r^2$, respectively. Q_{1i} couples with the charge at site i, $\rho_i = \Sigma_a C^{+}_{i,a} C_{i,a}$ whereas Q_{2i} and Q_{3i} couple with the x and z orbital pseudospin, $\tau_{xi} = C^{+}_{i1}C_{i2} + C^{+}_{i2}C_{i1}$ and $\tau_{zi} = C^{+}_{i1}C_{i1} - C^{+}_{i2}C_{i2}$, respectively. The third term is the elastic energy of the octahedra distortions, being $\beta \geqslant 2$ the spring constant ratio for breathing and JT modes.[38] In the perovskite structures the oxygens are shared by neighboring MnO_6 octahedra and the Q's distortions are not independent, cooperative effects being very important.[39] In order to consider these collective effects, we consider the position of the oxygen atoms as the independent variables of the JT distortions.

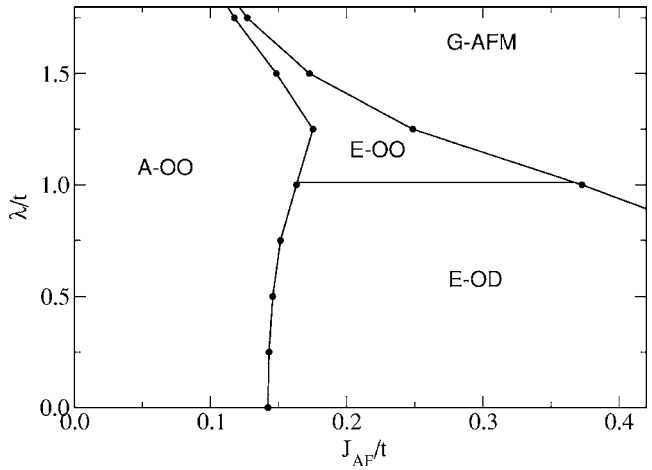

FIG. 1. Zero temperature phase diagram for $x=1$ for the two-dimensional DE two orbital model with cooperative Jahn-Teller phonons. The symbols OO and OD stand for orbital ordered and orbital disordered, respectively. A, E, and G name the different magnetic order defined in the text.

For a given value of the parameters λ and J_{AF}, and a texture of core spins $\{\mathbf{S}_i\}$, we solve self-consistently the mean field version of Hamiltonian (2) and obtain the energy, the local charges $\{\rho_i\}$, the orbital pseudospin order $\{\tau_{xi}, \tau_{zi}\}$ and the oxygen octahedra distortions $Q_{\alpha,i}$. These quantities are better described by their Fourier transforms, that are represented by the same symbol with a hat, $\hat{\rho}(\mathbf{G})$, $\hat{Q}_1(\mathbf{G}), \ldots$.

In Fig. 1 we present the phase diagram obtained by solving self-consistently Eq. (2) for the parent compound $R\mathrm{MnO}_3$. For the range of parameters studied, we do not find any solution showing charge modulation. In all the phases there is an electron located on each Mn ion, therefore in our model any gap in the energy spectrum is due to the spatial modulation of any other physical quantity.

For small values of J_{AF} the ground state is ferromagnetic, A-order. In absence of Jahn-Teller coupling this phase is metallic, however, for $\lambda \neq 0$, and due to the perfect nesting between the e_g bands, the A phase develops a gap at the Fermi energy. The Jahn-Teller coupling produces and orbital order characterized by a finite Fourier component of the x component of the pseudospin $\hat{\tau}_x(\pi,\pi) = \hat{\tau}_x(-\pi,-\pi) \neq 0$, see Fig. 2(a). The orbital order (OO) is produced by an ordered distribution of the oxygen octahedra distortions $\hat{Q}_2(\pi,\pi) = \hat{Q}_2(-\pi,-\pi) \neq 0$, that depends on the value of λ. The amplitude of the distortions are modulated in order to

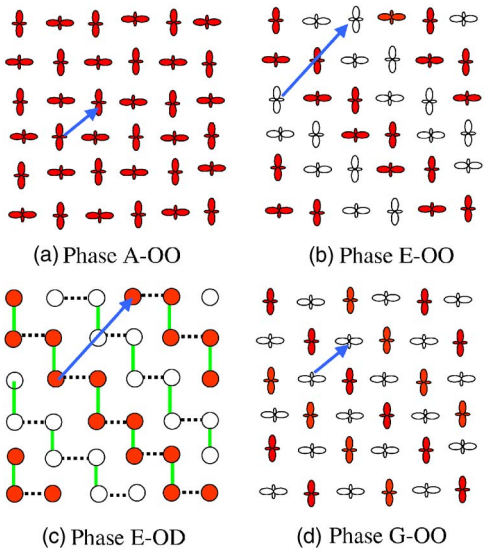

FIG. 2. (Color online) Orbital and spin order of $x=1$ manganites in the x-y plane. Elongated orbitals along the x (y) directions represent $d_{3x^2-r^2}$ ($d_{3y^2-r^2}$) orbitals. Circles represent the Mn ions in a orbital disordered phase. (a) Orbital order present in the ferromagnetic A-OO phase. (b) Same as (a) but for the E-OO phase. (c) Spin order in the E-OD phase. The solid and the dashed lines joining the Mn ions indicate the modulation of the electronic coherence along the zigzag chains. (d) Same as (a) but for the G-OO phase. In all the phases there is not modulation of the electric charge and there is an electron located at each Mn ion. The vectors in the different schemes, represent the spatial periodicity in the different phases, (a,a) in the A-OO and G-OO phases and $(2a,2a)$ in the E-OO and E-OD phases. In all the figures open and closed symbols represent up and down spins.

minimize the elastic energy of the cooperative Jahn-Teller distortions, and the signs arise from cooperative effects. In this phase the (π,π) orbital modulation opens a gap at the Fermi energy and the $x=1$ manganite is an insulator, being the energy gap proportional to the value of the Jahn-Teller coupling.

For large value of J_{AF} and λ the system presents a G-type antiferromagnetic ground state and an orbital order characterized by a Fourier component of the pseudospin $\hat{\tau}_x(\pi,\pi)=\hat{\tau}_x(-\pi,-\pi)\neq 0$. Each Mn ion is coupled antiferromagnetically with its next neighbors and the double exchange mechanism precludes the motion of the carriers, being this phase an insulator. The minimal value of J_{AF} for the occurrence of this phase depends on λ, but in general is very large, so that this phase is rather unlikely to occur in manganites.

For intermediates values of J_{AF} the system develops a magnetic order of E-type; the E phase consists of ferromagnetic zigzag chains coupled antiferromagnetically. The horizontal and vertical steps of the chain contain two Mn ions. For large enough values of the Jahn-Teller coupling the E magnetic order coexists with an orbital order similar to the one occurring in the A and G phases; this order opens a gap at the Fermi energy. In the E-OO phase the magnetic order is characterized by a periodicity $(2a,2a)$, being a the lattice parameter of the square lattice. For small values of λ the E phase does not present orbital order, although it has a gap at the Fermi energy. In the orbital disorder (OD) E phase, the dispersion energy for the e_g electrons along the FM zigzag chain is given by[32] $\varepsilon_k=(2/3)(\pm\cos k\pm\sqrt{\cos^2 k+3})$, indicating the existence of a large band gap at occupancies corresponding to $x=1$. The physical origin of this gap is the dependence of the tunnelling probability on the spatial direction, $t^x_{\mu,\nu}=-t^y_{\mu,\nu}$ for $\mu\neq\nu$. It produces a periodicity in the hopping amplitude along the zigzag chain, leading to a periodic potential for the e_g electrons. It is important to note that, contrary to the $x=1/2$ case,[14,15] this modulation in the hopping amplitude does not produce an orbital order. The E-OD phase is stable due to the spatial modulation of the coherence between next neighbors Mn ions along the zigzag chain, $\langle C^+_{i,\mu}C_{i+1,\nu}\rangle=-\langle C^+_{i+1,\mu}C_{i+2,\nu}\rangle$ for $\mu\neq\nu$. The phases E-OO and E-OD have different symmetry and therefore the transition between the phases that occurs at finite values of λ is a discontinuous transition.

These results are in accordance with Raman experiments. They show that orbital order exists for the orthorhombic A-type magnetically ordered samples, but disappears for hexagonal samples,[40] or when a ferromagnetic state is induced with a large magnetic field near the Curie temperature.[41] These experiments could clarify whether E-type magnetically ordered phases present orbital order.

III. FINITE TEMPERATURE MAGNETIC PHASE DIAGRAM

The simplest way of obtaining information on the phase diagram corresponding to a given microscopic Hamiltonian is by means of the mean field approximation. This approximation is insufficient for describing second order transitions, but it is successful in describing the phases away from the transition and in predicting the topology of the phase diagram. In this approach we compute the magnetic critical temperature of the different phases.

A. Ferromagnetic (A) phase

In this phase all the Mn spins point, on average, in a particular direction, and there is a finite relative magnetization $\langle m\rangle$. Using a virtual crystal approximation, we consider a unique value for the spin reduction factor $f_{i,j}$ that corresponds to its expectation value,[15,42]

$$f_{ij}\simeq\left\langle\sqrt{\frac{1+\cos\theta_{ij}}{2}}\right\rangle\simeq\sqrt{\frac{1+\langle\cos\theta_{ij}\rangle}{2}}=\sqrt{\frac{1+\langle m\rangle^2}{2}}. \tag{3}$$

A reduction of $\langle m\rangle$ produces a decrease in $f_{i,j}$ and therefore in the kinetic energy. In this way the importance of the Jahn-Teller coupling increases as the temperature decreases. The internal energy per Mn ion of this phase can be written as

$$E^A=\varepsilon_A(\lambda,\langle m\rangle)+2J_{\mathrm{AF}}\langle m\rangle^2, \tag{4}$$

where the electronic energy per Mn ion, $\varepsilon_A(\lambda,\langle m\rangle)$, depends in a complicated way on λ and $\langle m\rangle$ and must be obtained numerically by solving Eq. (2).

In order to describe thermal effects it is necessary to compute the free energy. As the entropy of the carriers is very small[14] we only include the entropy of the classical Mn spins. We use a mean field approximation that neglects spatial correlations and assume for each individual spin a statistical distribution corresponding to an effective magnetic field.[14,37] In this molecular field approximation the entropy of the Mn spins takes the form

$$S(\langle m\rangle) = \frac{\ln 2}{2} - \frac{3}{2}\langle m\rangle^2 - \frac{9}{20}\langle m\rangle^4 + \cdots . \tag{5}$$

Using this expression for the Mn spins entropy the total free energy of the system for small values of $\langle m\rangle$ takes the form

$$F(\langle m\rangle) = E^A - TS(\langle m\rangle)$$

and the Curie temperature of the A phase is

$$T_C = -\frac{2}{3}\left.\frac{\partial \varepsilon^A(\lambda,\langle m\rangle)}{\partial \langle m\rangle^2}\right|_{\langle m\rangle=0} - \frac{4}{3}J_{\mathrm{AF}}. \tag{6}$$

For finite λ the derivative must be calculated numerically. From higher derivatives of the internal energy with respect to the magnetization we obtain that the transition is second order. In Eq. (6) we notice that for a given value of the Jahn-Teller coupling the Curie temperature decreases linearly with the superexchange antiferromagnetic coupling J_{AF}.

B. Antiferromagnetic *E* phase

The magnetization of the E phase is described by the relative amount of saturation in each zigzag chain $\langle m_s\rangle$. In the virtual crystal approximation fluctuations are neglected and the hopping is modulated by the spin reduction factor that is different along the zigzag FM chain, f^{FM} than between the AFM coupled chains, f^{AF},[15,37]

$$f^{\mathrm{FM}}(\langle m_S\rangle) = \sqrt{\frac{1+\langle m_S\rangle^2}{2}},$$

$$f^{\mathrm{AF}}(\langle m_S\rangle) = \sqrt{\frac{1-\langle m_S\rangle^2}{2}}. \tag{7}$$

The internal energy of this phase depends on λ, and $\langle m_S\rangle$, and can be written as

$$E^E = \varepsilon_E(\lambda,\langle m_S\rangle). \tag{8}$$

As each Mn spin core is surrounded by two Mn spins coupled FM and other two coupled AFM, the superexchange energy is zero.

In order to compute the Néel temperature of the E phases, we introduce an effective field for each spin sublattice. Taking into account that both, the magnetization and the effective magnetic field, have a different sign in each sublattice, we end up with the same expression for the entropy than in the A phase, but just changing $\langle m\rangle$ by $\langle m_S\rangle$.[15] With this the free energy takes the form

$$\begin{aligned} F(\langle m_S\rangle,\lambda) &= E^E - TS(\langle m_S\rangle) \\ &\simeq F(0,\lambda) + \langle m_S\rangle^2\left(\tfrac{3}{2}T + a\right) + \langle m_S\rangle^4\left(\tfrac{9}{20}T + b\right) \\ &\quad + \langle m_S\rangle^6\left(\tfrac{99}{350}T + c\right) + \cdots \end{aligned} \tag{9}$$

with

$$E^E \approx cte + a\langle m_S\rangle^2 + b\langle m_S\rangle^4 + c\langle m_S\rangle^6 + \cdots . \tag{10}$$

Due to the symmetry of the E phase the coefficient a is zero, and the Néel temperature depends on the coefficients b and c. Numerically, the coefficient b is negative and the transition from the E to the paramagnetic (PM) phase is a first order phase transition.

It is interesting to analyze the origin of the negative sign of the quartic term. In the OD case the Jahn-Teller coupling is not large enough to produce orbital order. In this situation the electronic energy is just kinetic energy. Therefore near $\langle m_S\rangle = 0$ we would expect that the electronic energy could be obtained perturbatively from the paramagnetic energy as $E^E_{\lambda=0} \approx (1/\sqrt{2})[f^{\mathrm{FM}}(\langle m_S\rangle) + f^{\mathrm{AF}}(\langle m_S\rangle)]\varepsilon^0_E$. Here $\varepsilon^0_E \equiv \varepsilon_E(0,0)$ is the paramagnetic energy per Mn ion. Expanding the spin reduction factors near $\langle m_S\rangle$ we find $E^E_{\lambda=0} \approx \left(1 - \frac{1}{8}\langle m_S\rangle^4 - \frac{5}{128}\langle m_S\rangle^8 - \cdots\right)\varepsilon^0_E$. As the electronic energy of the paramagnetic phase is negative, the last expression suggests that the Néel temperature should be zero. However, numerically, we find a finite Néel temperature even for $\lambda = 0$. This discrepancy occurs because, as commented above, in the E-OD phase the minimization of the kinetic energy produces a modulation of the electron coherence along the zigzag chain, $\langle C^+_{i,\mu}C_{i+1,\nu}\rangle = -\langle C^+_{i+1,\mu}C_{i+2,\nu}\rangle$ for $\mu \neq \nu$. We describe this modulation by a order parameter ξ that represents the $(\pi/2,\pi/2)$ Fourier component of the electron coherence. This order parameter is coupled with the staggered magnetization and the functional describing the electronic energy has the general form

$$E^E_{\lambda=0}\frac{1}{\sqrt{2}}[f^{\mathrm{FM}}(\langle m_S\rangle) + f^{\mathrm{AF}}(\langle m_S\rangle)]\varepsilon^0_E + \alpha\xi^2 + \beta\xi\langle m_S\rangle^2 + \cdots , \tag{11}$$

where we have included the elastic energy associated with the electron coherence and the minimal coupling between the staggered magnetization and the electron coherence. Minimizing this energy with respect to the coherence parameter ξ, we find $\xi = -(\beta/2\alpha)\langle m_S\rangle^2$. Introducing this value in the expression of the electronic energy, Eq. (11), we obtain

$$E^E_{\lambda=0} \approx \left(1 - \frac{1}{8}\langle m_S\rangle^4\right)\varepsilon^0_E - \frac{\beta^2}{4\alpha}\langle m_S\rangle^4 + \cdots \tag{12}$$

and for strong enough coupling between $\langle m_S\rangle$ and the orbital coherence, the quartic term is negative and a finite Néel temperature is expected. It is therefore the coupling between the electron coherence and the staggered magnetization that are responsible for the occurrence of a finite Néel temperature.

In the OO case there exists a finite orbital order parameter $\hat{\tau}_x(\pi,\pi)$, that is coupled with the staggered magnetization and it is responsible for the existence of finite Néel temperature.

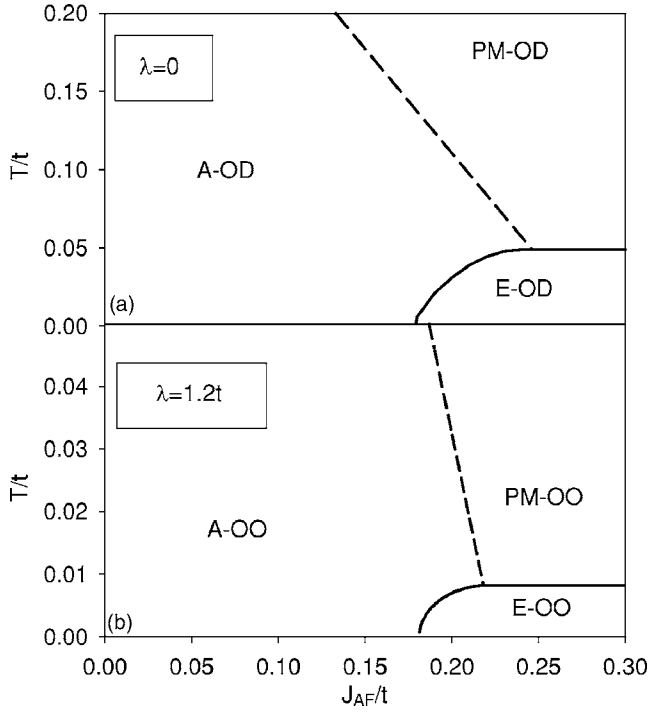

FIG. 3. Phase diagrams T-J_{AF} for the two-dimensional DE two orbital model with cooperative Jahn-Teller phonons and $x=1$. In (a) we plot the $\lambda=0$ case and in (b) the $\lambda=1.2t$ case. Continuous lines represent first order transitions whereas dashed lines indicate second order transitions. The abbreviations naming the different phases are explained in the text.

C. Temperature-J_{AF} magnetic phase diagram

In Fig. 3, we plot the T-J_{AF} magnetic phase diagrams for $\lambda=0$ (a) and $\lambda=1.2t$ (b). These phase diagrams have been obtained by minimizing and comparing the free energy of the A, E, and paramagnetic phases. For $\lambda=0$, all the phases are disordered in the orbital sector, however, for large enough values of λ, the E and A phases present orbital order. In the latter case, $\lambda=1.2t$, we find that the critical temperature associated with the orbital order is much larger than the magnetic critical temperatures and, therefore, in Fig. 3(b) the paramagnetic phase presents orbital order. In any case, it is important to note that, from the magnetic point of view, both phase diagrams are topologically equivalent. At large temperatures the systems are always paramagnetic, for small J_{AF} and small temperature the systems present ferromagnetic order, whereas for small temperature and moderate values of J_{AF} an antiferromagnetic order of type E appears. For very large values of the AFM coupling, not shown in Fig. 3, antiferromagnetic order of type G would appear. The Curie temperature corresponding to the paramagnetic-A phase transition decreases linearly with J_{AF}, Eq. (6), until it reaches the, J_{AF} independent, Néel temperature corresponding to the paramagnetic-E transition. As discussed in the preceding section the A-paramagnetic transition is second order while, because of the coupling between different order parameters, the E-paramagnetic transition is first order.

The phase diagrams present a Lifshitz point where the uniform ferromagnetic A phase, the modulated ordered E phase and the paramagnetic disordered phase meet. Near the Lifshitz point there is a range of values of J_{AF} where, by increasing the temperature, the system undergoes an E-A transition followed by an A-PM transition. The topology of this phase diagram is similar to that of a Ising model with competing interactions. In that model, near the Lifshitz point, solitons, spatially modulated phases and commensurate-incommensurate transitions appear when the temperature varies.[31] In the next section we explore the possible existence of solitons and incommensurate phases in the model described by the Hamiltonian Eq. (2) at $x=1$ and near the Lifshitz point that appears in the T-J_{AF} phase diagram, Fig. 3.

IV. SOLITON THEORY AND SPATIALLY MODULATED PHASES

A. Landau functional

Magnetically, the phases described in the preceding sections only vary along the direction perpendicular to the chains, see Fig. 2. In the mean field approximation the E phase is described by a spin density wave of the form $\langle S\rangle=\sqrt{2}m_0\cos(q_0z+\pi/4)$, with $q_0=\pi/2$ and here z is the position of the atoms along the direction perpendicular to the chains. We are taking the distance between first neighbors diagonal lines of atoms, $\sqrt{2}a/2$, as the unit of length. In general the expression

$$\langle S\rangle=\sqrt{2}m_0\cos\left(q_0z+\frac{\pi}{4}+\theta(z)\right) \tag{13}$$

describes different spatially modulated magnetic phases. With $\theta(z)=0$ it describes the E phase, whereas with $\theta(z)=-q_0z$, it represents the average magnetization in the position independent ferromagnetic A phase. The case $m_0=0$ corresponds to the paramagnetic case. In general $\theta(z)$ describes phases where the average magnetization changes along the direction perpendicular to the chains. (see Fig. 4.)

Both the E and A phases are commensurate with the underlying lattice, here we are going to study the existence of solitons and incommensurate phases in the system. The solitons are static domain walls between commensurate domains. In this section we present a formalism which makes contact with phenomenological theories and provides the basis for the calculation of the nature of the phase diagram at finite temperature.

We want to build a Landau theory functional where the order parameter is the modulation of the average spin along the diagonal direction. Following Refs. 43 and 44, in Eq. (13) we consider the amplitude of the magnetization, m_0, as constant in the space.

In order to set up a Landau theory we need to calculate the different contributions to the free energy. For a magnetization given by Eq. (13), and near the order-disorder magnetic transitions, the entropic contribution to the free energy can be estimated as described in Sec. III,

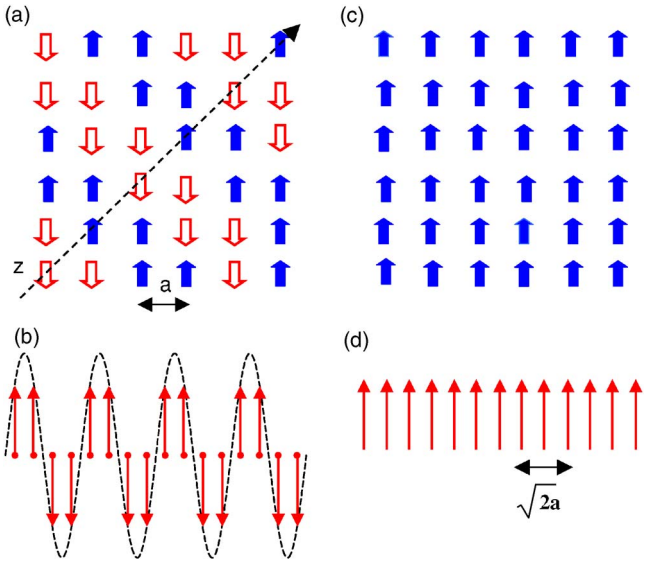

FIG. 4. (Color online) Spin order of $x=1$ manganites in the x-y plane. (a) corresponds to the E phase whereas (c) represents the A phase. The direction perpendicular to the zigzag chains is shown in (a). The averaged magnetization along the z direction for the E and A phases are plotted in (c) and (d), respectively.

$$-TS \simeq k_B T \int \left[-\ln 2 + \frac{3}{2} m_0^2 + \frac{27}{40} m_0^4 + \frac{99}{140} m_0^6 - \left(\frac{9}{40} m_0^4 + \frac{297}{700} m_0^6 \right) \cos 4\theta(z) \right] dz. \tag{14}$$

The superexchange antiferromagnetic interaction takes the form

$$E_{\mathrm{AF}} \simeq 2 J_{\mathrm{AF}} m_0^2 \int \sin[\nabla \theta(z)] dz, \tag{15}$$

where $\nabla\theta(z)$ is the derivative of $\theta(z)$ with respect to z. In the previous expression we have treated the position z as a continuous variable and we have discarded second and higher derivatives of θ with respect to the position.

Concerning the electronic contribution to the internal energy, E_e, we assume that it is local and can be written as $E_e = \int dz \mathcal{E}(z)$, being $\mathcal{E}(z)$ the electronic energy density. We expect that it can be expanded in powers of the order parameter $\langle S \rangle$ and its derivatives,

$$\mathcal{E}(z) = \mathcal{E}^0 + \tilde{a}_l(z) \langle S(z) \rangle^l + \tilde{b}_l(z) [\nabla \langle S(z) \rangle]^l + \tilde{c}_{l,m}(z) \times \langle S(z) \rangle^l [\nabla \langle S(z) \rangle]^m \cdots . \tag{16}$$

Here the sum over repeated indices is assumed, and because the symmetry of the system only even powers of $\langle S \rangle$ and $\nabla \langle S(z) \rangle$ contribute. The coefficients $\tilde{a}_l$, $\tilde{b}_l$, and $\tilde{c}_{l,m}$ are periodic in z with the periodicity of the crystal lattice and for a magnetization of the form Eq. (13), the density of electronic energy can be written as

$$\mathcal{E}(z) = \mathcal{E}^0 + a_2 m_0^2 + a_4 m_0^4 + a_6 m_0^6 + (b_4 m_0^4 + b_6 m_0^6) \cos 4\theta(z) + (c_2 m_0^2 + c_4 m_0^4 + c_6 m_0^6) [\nabla \theta(z) + q_0]^2. \tag{17}$$

Here we have neglected higher terms in the derivates of the phase θ and, as there are first order phase transitions in some part of the phase diagram, we keep terms up to the sixth power in m_0. The second term in Eq. (17) is the Umklapp term that favors the modulated commensurate solutions, $\theta(z) = 0, \pi/2, \pi, 3(\pi/2)$, corresponding to the E phase. The last term is an elastic energy which favors the occurrence of the ferromagnetic A phase, $\theta(z) = -q_0 z$. The competition between the elastic and the Umklapp will produce the existence of solitons and incommensurate phases.

From the expression of the electronic energy of the E phase as a function of the order parameter m_0, we notice $a_2 = -c_2 q_0^2$. Analyzing the dependence of the electronic energy on a constant phase $[\theta(r) = \theta_0]$, we find $b_4 = a_4 + c_4 q_0^4$ and $b_6 = a_6 + c_6 q_0^4$. In this way only two subsets of parameters (for instance b's and c's) are independent. Finally, for each value of λ, we perform microscopic calculations of the electronic energy of the A and E phases and obtain the numerical values of the coefficients b's and c's respectively.

Adding the entropy, Eq. (14), the antiferromagnetic energy, Eq. (15) and the electronic internal energy, Eq. (17), we obtain the following expression for the free energy of the system:

$$F = F_0(T, m_0) + C \int \left(\frac{1}{2} [\nabla \theta(z) + q_0]^2 + w[1 + \cos 4\theta(z)] \right) dz, \tag{18}$$

with

$$F_0(T, m_0) = \left(-\ln 2 + \tfrac{3}{2} m_0^2 + \tfrac{9}{10} m_0^4 + \tfrac{198}{175} m_0^6 \right) T - 2 J_{\mathrm{AF}} m_0^2 + \varepsilon_e^0 - c_2 m_0^2 q_0^2, \tag{19}$$

$$C = \left(2c_2 + 4 \frac{J_{\mathrm{AF}}}{q_0^2} \right) m_0^2 + 2 c_4 m_0^4 + 2 c_6 m_0^6, \tag{20}$$

and

$$w = \frac{\left(b_4 - \frac{9}{40} \right) m_0^4 + \left(b_6 - \frac{297}{700} T \right) m_0^6}{C}. \tag{21}$$

In the limit $w \to 0$, the elastic contribution is the more important term and the phase $\theta(z)$ tends to be $\theta(z) = -q_0 z$. On the contrary, for large values of w, the Umklapp term is dominant and θ wants to get a constant value, $\theta = 0, \pi/2, \pi, 3(\pi/2)$. A transition between the commensurate phase, $\theta = 0$ and the uniform ferromagnetic phase takes place because of the competition between these two terms; by tuning the values of J_{AF} and T we are going to see that a soliton incommensurate phase appears between these two limits.

For a given temperature and a particular value of J_{AF}, the constant amplitude m_0 and the phase function $\theta(z)$ that characterize the solution are obtained by minimizing the functional Eq. (18). For each m_0, the phase $\theta(z)$ should satisfy the sine-Gordon equation,

$$\frac{1}{2}\frac{d^2\theta}{dz^2} + 4w \sin 4\theta = 0 \tag{22}$$

which has solitonlike solutions of the form

$$\theta(z) = \tan^{-1} \exp(4\sqrt{w}z). \tag{23}$$

This solution is a domain wall which separates two almost commensurate z regions.

In general the solution of Eq. (18) is a soliton lattice formed by a regular array of domain walls, L. At each soliton the phase θ tumbles $\pi/2$. The deviation of the average wave vector $\bar{q}$ from q_0 is inversely proportional to the distance, L, between the domain walls,

$$\bar{q} = \frac{\pi}{2L}. \tag{24}$$

The value of $\bar{q}$ is proportional to the soliton density and is obtained by minimizing the free energy following the procedure outlined in Refs. 31 and 43–45.

In the soliton lattice phase the magnetic periodicity along the z direction is characterized by the wave vector

$$q = \frac{\pi}{2} - \frac{\pi}{2L}. \tag{25}$$

In the E phase there are not solitons in the system, $L=\infty$, and the wave vector of the magnetic modulation is $q=\pi/2$. In the continuous approximation the ferromagnetic A phase corresponds to a extremely dense lattice soliton, $L=1$. In this limit, θ is too quickly varying, the continuous approximation is not valid, and we take the criterium that for $L \leqslant 1.1$, the soliton lattice is the ferromagnetic A phase.

B. Results

In order to find inhomogeneous phases in manganites at $x=1$, we have minimized the free energy Eq. (18) with the coefficients a's, b's, and c's obtained from the microscopic model described in Sec. II. The solutions are characterized by the value of the magnetization m_0 and the density of solitons $\bar{q}$. We present results for the case $\lambda=0$, but similar results are obtained for finite Jahn-Teller coupling.

If we consider only the uniform solutions, E and A phases, the minimization of the free energy results in the phase diagrams already presented in Sec. III, Fig. 3. When inhomogeneous solutions are considered, we obtain the phase diagram shown in Fig. 5. Several comments on this phase diagram are in order: (i) There are not solitons for values of J_{AF} larger than the antiferromagnetic coupling corresponding to the Lifshitz point. The paramagnetic-E phase transition is first order, with a large jump in the value of m_S, and therefore in the value of w. In this situation, large values of w, the Umklapp term is much stronger than the elastic term and the system prefers to be commensurate with the lattice. Note than in the paradigmatic Ising model with competing interactions[31] all the transitions are second order and incommensurate phases appear at both sides of the Lifshitz point. (ii) For small values of J_{AF} the elastic term is very strong and the solution corresponds to a dense soliton phase.

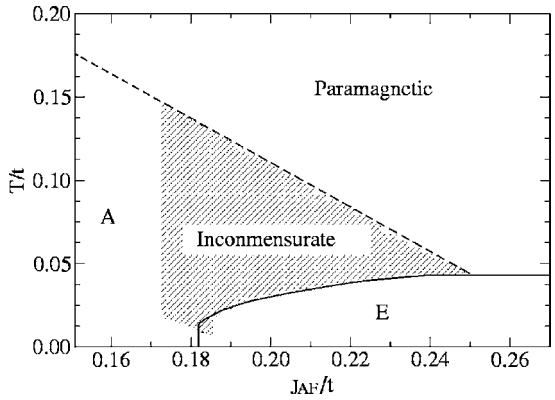

FIG. 5. Phase diagram T-J_{AF} as obtained by minimizing the free energy Eq. (18). The parameters of entering in the free energy are obtained by minimizing the microscopic Hamiltonian Eq. (2) for $\lambda=0$ and $x=1$. Continuous lines represent first order transitions whereas dashed lines indicate second order transitions. The shadow region indicates the region where the incommensurate phase exits.

For small values of J_{AF} the distance between solitons is smaller than the cutoff and we consider that this commensurate phase is actually, in the discrete real crystal, the ferromagnetic A phase. (iii) For intermediate values of J_{AF}, the competition between the elastic and the Umklapp term results in the appearance of incommensurate solitonic phases.

In Fig. 5, the shadow region indicates the incommensurate phase. The frontier of this phase with the ferromagnetic A phase is diffuse because, as we have already discussed, to distinguish between a dense soliton phase and the ferromagnetic A phase we take a criterion based on the distance between solitons. Although experiments in Tb and Dy compounds show lock-in transition to incommensurate phases at low temperature,[29] we have not found solitonic phases in the zero T limit of the Ginburz-Landau functional. Neither have we found stable solitons by diagonalizing the microscopic Hamiltonian, Eq. (2). A recent work including ferroelectric couplings[46] might clarify this issue. Typical temperature dependence of the magnetic wave vector and magnetization amplitude near the incommensurate phase is illustrated in Fig. 6. For low temperature the system is in the commensurate E phase, corresponding to a wave vector $q=\pi/2$. At low temperatures the spins are highly polarized and that makes the magnetic modulation too rigid to allow solitons. As temperature increases, the amplitude of the spin modulation, m_0 decreases and, at a J_{AF} dependent temperature, a jump to the solitonic phase takes place. For values of J_{AF} closer to the Lifshitz point, the incommensurate phase appears at temperatures near the A-paramagnetic critical temperature. In that case the amplitude of the magnetization m_0 is small and hence the magnetic wave vector of the incommensurate phase is also very small. Therefore, in this part of the phase diagram the incommensurate phase is similar to the A phase.

For values of J_{AF} near the zero temperature A to E phase transition, there is a small portion of the phase diagram where, by decreasing the temperature, the system evolves first from a paramagnetic, $q=0$, phase to a incommensurate phase characterized by a finite q, and then to a ferromagnetic A phase without magnetic modulation, $q=0$.

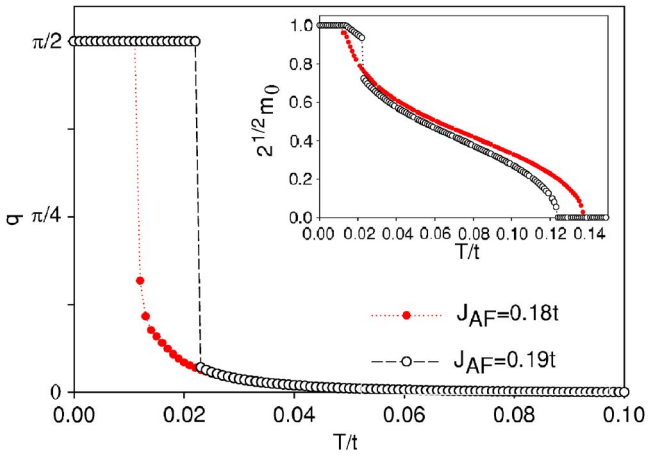

FIG. 6. (Color online). Temperature dependence of the magnetic wave vector, q, and of the order parameter amplitude, m_0 (inset), for two values of J_{AF}. The wave vector $q=\pi/2$ corresponds to the E phase and $q=0$ to the A phase. The results are obtained by minimizing the free energy [Eq. (18)].

The magnetic phase diagram shown in Fig. 5 contains the essence of the magnetic properties experimentally observed in undoped manganites.[29] Systems with large hopping amplitude (J_{AF}/t small) as $LaMnO_3$ have a ground state with a magnetic order of type A and a relatively large Néel temperature. The relative value of the AFM coupling increases when the ionic radius of the rare earth in the manganite increases. Therefore we understand the experimental decrease of the Néel temperature in the series of $RMnO_3$ (R =La,Pr,Nd,Sm) as the diminution of the A-paramagnetic critical temperature when J_{AF} increases, see Figs. 3 and 5. Experimentally it is observed that for large enough ionic radius, $HoMnO_3$, the ground state of the undoped manganite has a magnetic order of type E, and present incommensurate phases when temperature increases. We claim that this situation corresponds in the phase diagram Fig. 5 to values J_{AF}/t in the range 0.18–0.20. Experimentally it is also observed that in some compounds as $TbMnO_3$ and $GdMnO_3$, when the temperature increases, the system undergoes two phase transitions, first a a ferromagnetic-incommensurate transition and, at higher temperatures, a incommensurate-paramagnetic transition. In the phase diagram presented in Fig. 5 similar behavior occurs for values of J_{AF} near $0.18t$.

V. SUMMARY

By starting from a microscopic Hamiltonian we have derived an expression for the free energy of undoped manganites. Using a realistic model, we have quantified the competition between the short range superexchage antiferromagnetic interaction, and the long range double exchange ferromagnetic interaction. The competition between these interactions results in the existence of magnetic incommensurate phases as recently experimentally observed in undoped manganites. The incommensurate phases can be described as arrays of domain walls separating commensurate phases by a distance that depends on temperature. The results presented in Fig. 5 explain qualitatively the experimental results presented in Ref. 29.

ACKNOWLEDGMENTS

Financial support is acknowledged from Grant No. MAT2002-04429-C03-01 (MCyT, Spain).

[1] Y. Tokura, J. Magn. Magn. Mater. **200**, 1 (1999).
[2] N. Furukawa, in *Physics of Manganites*, edited by T. Kaplan and S. Mahanti (Kluwer/Plenum, New York, 1999).
[3] E. Dagotto, *Nanoscale Phase Separation and Colossal Magnetoresistance* (Springer-Verlag, Berlin, 2002).
[4] J. B. Goodenough, Phys. Rev. **100**, 564 (1955).
[5] P. G. Radaelli, D. E. Cox, M. Marezio, and S.-W. Cheong, Phys. Rev. B **55**, 3015 (1997).
[6] Y. Tomioka and Y. Tokura, Phys. Rev. B **66**, 104416 (2002).
[7] F. Rivadulla, E. Winkler, J.-S. Zhou, and J. B. Goodenough, Phys. Rev. B **66**, 174432 (2002).
[8] A. Daoud-Aladine, J. Rodriguez-Carvajal, L. Pinsard-Gaudart, M. T. Fernańdez-Díaz, and A. Revcolevschi, Phys. Rev. Lett. **89**, 097205 (2002).
[9] S. P. Greiner, J. P. Hill, D. Gibbs, K. J. Thomas, M. v. Zimmermann, C. S. Nelson, V. Kiryukhin, Y. Tokura, Y. Tomioka, D. Casa, T. Gog, and C. Venkataraman, Phys. Rev. B **69**, 134419 (2004).
[10] I. V. Solovyev and K. Terakura, Phys. Rev. Lett. **83**, 2825 (1999).
[11] J. van den Brink, G. Khaliullin, and D. Khomskii, Phys. Rev. Lett. **83**, 5118 (1999).
[12] V. Ferrari, M. Towler, and P. B. Littlewood, Phys. Rev. Lett. **91**, 227202 (2003).
[13] M. J. Calderón, A. J. Millis, and K. H. Ahn, Phys. Rev. B **68**, 100401(R) (2003).
[14] L. Brey, Phys. Rev. Lett. **92**, 127202 (2004).
[15] L. Brey, Phys. Rev. B **71**, 174426 (2005).
[16] M. Uehara, S. Mori, C. H. Chen, and S.-W. Cheong, Nature (London) **399**, 560 (1999).
[17] C. H. Chen and S.-W. Cheong, Phys. Rev. Lett. **76**, 4042 (1996).
[18] J. C. Loudon, S. Cox, A. J. Williams, J. P. Attfield, P. B. Littlewood, P. A. Midgley, and N. D. Mathur, Phys. Rev. Lett. **94**, 097202 (2005).
[19] G. Milward, M. Calderon, and P. Littlewood, Nature (London) **433**, 607 (2005).
[20] L. Brey and P. B. Littlewood, Phys. Rev. Lett. **95**, 117205 (2005).
[21] T. Mizokawa and A. Fujimori, Phys. Rev. B **54**, 5368 (1996).
[22] R. Maezono, S. Ishihara, and N. Nagaosa, Phys. Rev. B **57**, R13993 (1998).
[23] J. van den Brink, P. Horsch, F. Mack, and A. M. Oleś, Phys. Rev. B **59**, 6795 (1999).
[24] L. F. Feiner and A. M. Oleś, Phys. Rev. B **59**, 3295 (1999).
[25] M. Capone, D. Feinberg, and M. Grilli, Eur. Phys. J. B **17**, 103 (2000).

[26] K. H. Ahn and A. J. Millis, Phys. Rev. B **64**, 115103 (2001).
[27] E. T. Seppala, A. M. Pulkkinen, and M. J. Alvala, Phys. Rev. B **66**, 144403 (2002).
[28] A. Muñoz, M. T. Casáis, J. A. Alonso, M. J. Martínez-Lope, J. L. Martínez, and M. T. Fernández-Díaz, Inorg. Chem. **40**, 1020 (2001).
[29] K. Kimura, S. Ishihara, H. Shintani, T. Arima, K. T. Takahashi, K. Ishizaka, and Y. Tokura, Phys. Rev. B **68**, 060403(R) (2003).
[30] R. Kajimoto, H. Yoshizawa, H. Shintani, T. Kimura, and Y. Tokura, Phys. Rev. B **70**, 012401 (2004).
[31] P. Bak and J. von Boehm, Phys. Rev. B **21**, 5297 (1980).
[32] T. Hotta, M. Moraghebi, A. Feiguin, A. Moreo, S. Yunoki, and E. Dagotto, Phys. Rev. Lett. **90**, 247203 (2003).
[33] T. Hotta, Phys. Rev. B **67**, 104428 (2003).
[34] D. V. Efremov and D. I. Khomskii, cond-mat/0407656 (unpublished).
[35] C. Zener, Phys. Rev. **82**, 403 (1952).
[36] P. Anderson and H. Hasewaga, Phys. Rev. **100**, 675 (1955).
[37] P.-G. de Gennes, Phys. Rev. **118**, 141 (1960).
[38] H. Aliaga, D. Magnoux, A. Moreo, D. Poilblanc, S. Yunoki, and E. Dagotto, Phys. Rev. B **68**, 104405 (2003).
[39] J. A. Vergés, V. Martín-Mayor, and L. Brey, Phys. Rev. Lett. **88**, 136401 (2002).
[40] L. Martin-Carron, A. de Andres, M. J. Martinez-Lope, M. T. Casais, and J. A. Alonso, J. Alloys Compd. **323**, 484 (2001).
[41] H. L. Liu, S. Yoon, S. L. Cooper, S. W. Cheong, P. D. Han, and D. A. Payne, Phys. Rev. B **58**, R10115 (1998).
[42] D. P. Arovas, G. Gómez-Santos, and F. Guinea, Phys. Rev. B **59**, 13569 (1999).
[43] W. L. McMillan, Phys. Rev. B **14**, 1496 (1976).
[44] W. L. McMillan, Phys. Rev. B **16**, 4655 (1977).
[45] P. G. DeGennes, Solid State Commun. **6**, 163 (1968).
[46] I. A. Sergienko and E. Dagotto, cond-mat/0508075 (unpublished).